A Bayesian-Based System to Assess Wave-Driven Flooding Hazards on Coral Reef-Lined Coasts

S. G. Pearson[1,2] (iD), C. D. Storlazzi[3] (iD), A. R. van Dongeren[1] (iD), M. F. S. Tissier[2] (iD), and A. J. H. M. Reniers[2]

[1]Department of Applied Morphodynamics, Unit of Marine and Coastal Systems, Deltares, Delft, the Netherlands, [2]Faculty of Civil Engineering and Geosciences, Delft University of Technology, Delft, the Netherlands, [3]Pacific Coastal and Marine Science Center, U.S. Geological Survey, Santa Cruz, CA, USA

Abstract Many low-elevation, coral reef-lined, tropical coasts are vulnerable to the effects of climate change, sea level rise, and wave-induced flooding. The considerable morphological diversity of these coasts and the variability of the hydrodynamic forcing that they are exposed to make predicting wave-induced flooding a challenge. A process-based wave-resolving hydrodynamic model (XBeach Non-Hydrostatic, "XBNH") was used to create a large synthetic database for use in a "Bayesian Estimator for Wave Attack in Reef Environments" (BEWARE), relating incident hydrodynamics and coral reef geomorphology to coastal flooding hazards on reef-lined coasts. Building on previous work, BEWARE improves system understanding of reef hydrodynamics by examining the intrinsic reef and extrinsic forcing factors controlling runup and flooding on reef-lined coasts. The Bayesian estimator has high predictive skill for the XBNH model outputs that are flooding indicators, and was validated for a number of available field cases. It was found that, in order to accurately predict flooding hazards, water depth over the reef flat, incident wave conditions, and reef flat width are the most essential factors, whereas other factors such as beach slope and bed friction due to the presence or absence of corals are less important. BEWARE is a potentially powerful tool for use in early warning systems or risk assessment studies, and can be used to make projections about how wave-induced flooding on coral reef-lined coasts may change due to climate change.

Plain Language Summary Low-lying tropical coasts fronted by coral reefs are threatened by the effects of climate change, sea level rise, and flooding caused by waves. However, the reefs on these coasts differ widely in their shape, size, and physical characteristics; the wave and water level conditions affecting these coastlines also vary in space and time. These factors make it difficult to predict flooding caused by waves along coral reef-lined coasts. We created a system ("BEWARE") that estimates how different wave, water level, and reef combinations can lead to flooding. This tool tells us what information is needed to make good predictions of flooding. We found that information on water levels and waves is most important, followed by the width of the reef. BEWARE can be used to make short-term predictions of flooding in early warning systems, or long-term predictions of how climate change will affect flooding caused by waves on coral reef-lined coasts.

1. Introduction

Thousands of reef-lined tropical islands are threatened by climate change, sea level rise, and coral degradation (Ferrario et al., 2014). Many of these islands, such as atolls, have low (<4 m above MSL) maximum elevations, making them particularly vulnerable to sea level rise and the impact of wave-driven flooding. For instance, on the Gilbert, Marshall, Caroline, and Maldives island chains, over 90% of the population and land area are located within 5 m of mean sea level (UN-Habitat, 2015). On many low-lying coral atolls, freshwater is constrained to a relatively thin (<15 m) freshwater lens. These aquifers are susceptible to wave-driven flooding that salinizes the freshwater lens, making the water unsuitable for human consumption (Gingerich et al., 2017; Terry & Falkland, 2010). For example, large storm-driven wave events occurring in 2008, 2009, and 2011 that coincided with high tides destroyed crops, demolished infrastructure, and contaminated freshwater drinking supplies on numerous atolls in the Pacific Ocean (Fletcher & Richmond, 2010; Hoeke

et al., 2013; U.S. Fish and Wildlife Service, 2015), underscoring the evident vulnerability of these reef-lined island communities. Even on more mountainous tropical islands, the majority of housing, critical infrastructure, and agriculture are situated on narrow coastal plains close to sea level. The susceptibility of these tropical islands to changing oceanic and climatic conditions represents a severe threat to food and water security, public safety, and environmental health.

Wave-driven flooding hazards on coral reef-lined islands not only result from large tropical cyclones but more commonly are the result of remotely generated ("sunny-day") swell events (Hoeke et al., 2013). When these waves or those from tropical cyclones encounter a reef-lined coast, they usually undergo significant transformation due to the abrupt changes in bathymetry. Through wave breaking and bottom friction dissipation, incident wave heights are reduced on the order of 90–99%, depending on the tidal stage (Ferrario et al., 2014; Péquignet et al., 2011). However, not all of this incident sea-swell wave energy ("SS," >0.04 Hz) is dissipated, and some is transferred to infragravity ("IG," 0.004–0.04 Hz) and very low frequencies ("VLF," <0.004 Hz), generally via the breakpoint mechanism/dynamic setup on the steep fore reef slope (Pomeroy et al., 2012b; Symonds et al., 1982). As a result, low-frequency wave energy often dominates at the shoreline, which promotes higher runup and hence an increased chance of flooding (Beetham et al., 2015; Cheriton et al., 2016; Gawehn et al., 2016; Roeber & Bricker, 2015; Shimozono et al., 2015).

Resonant amplification occurs when the highly energetic IG and VLF wave frequencies on the reef flat coincide with the nth natural frequency of the reef (f_n):

$$f_n = \frac{(2n+1)\sqrt{gh_{reef}}}{4W_{reef}}$$

(1)

where n is mode number, g is gravitational acceleration, h_{reef} is the mean water depth on the reef flat, and W_{reef} is the width of the reef flat. This phenomenon is controlled by parameters characterizing the reef (e.g., morphology) and extrinsic hydrodynamic forcing (Cheriton et al., 2016; Gawehn et al., 2016; Péquignet et al., 2009). The consequences of resonant amplification are dire because higher water levels can be excited on the reef flat than might be expected for the incident wave conditions, resulting in flooding or damage to coastal infrastructure (Nakaza et al., 1990; Péquignet et al., 2009; Roeber & Bricker, 2015; Tajima et al., 2016).

Vulnerability to wave-induced flooding is spatially heterogeneous due to the highly variable morphology of reef-lined coasts. Quataert et al. (2015) found that relatively smooth, deep, narrow reef flats fronted by steep fore reefs are prone to higher runup and therefore increased flood risk than other coral reef morphologies. Furthermore, Owen et al. (2016) noted that small variations in island topography and land use also influence wave-driven flooding and associated impacts. Therefore, the timing and severity of wave-induced impacts depend, in part, on island characteristics, but the uncertainty regarding the spatially variable shoreline morphology contributes considerable uncertainty to the prediction of these impacts. The vulnerability of Small Island Developing States to natural hazards is further enhanced by their small physical size, relative isolation, often limited resources (Meheux et al., 2007), and existing socioeconomic vulnerabilities (Ferrario et al., 2014). These vulnerabilities will likely increase in years to come due to population growth and climate-change effects such as sea level rise (Hinkel et al., 2014; Nicholls & Cazenave, 2010). All these factors may affect the habitability of these islands in the next century, displacing their people and causing internal migration or emigration. Indeed, Storlazzi et al. (2015) project that many atolls may become uninhabitable within the next few decades, when the recurrence interval of catastrophic floods becomes shorter than the recovery period for freshwater lenses, vegetation, wildlife populations, and repair of critical infrastructure. To combat threats like these, United Nations-endorsed Sendai Framework for Disaster Risk Reduction calls for improved access to early warning systems and disaster risk assessments by 2030 (UNISDR, 2015).

To answer this call and plan suitable adaptations, there is a need to improve how we evaluate and predict wave-driven flooding threats to these regions, which constitute a large, diverse set of islands and reef morphologies, all subject to a range of offshore oceanographic conditions. Bayesian networks are probabilistic models that have been successfully used to make predictions of hydrodynamics and morphology in numerous coastal applications (Gutierrez et al., 2011, 2015; Plant & Holland, 2011; Poelhekke et al.,
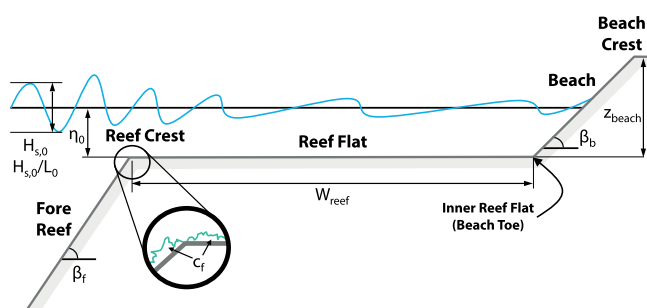
Figure 1. The idealized reef profile modeled in XBeach-Non-Hydrostatic with the relevant hydrodynamic and morphological parameters indicated: offshore water level with respect to the reef flat (η_0), offshore significant wave height (H_0), wave steepness (H_0/L_0), fore reef slope (β_f), bed roughness (c_f), reef width (W_{reef}), beach slope (β_f), and beach crest elevation (z_{beach}).

2016). They do not require a detailed description of the physical processes, as they only investigate the correlations between each variable. Hirschberg et al. (2011) call for a probabilistic approach for hydrometeorological forecasts, making Bayesian networks fit-for-purpose, since they handle the uncertainty inherent to climate change and short-term meteorologic-oceanographic processes. While process-based model simulations can be time consuming, Bayesian networks compile and provide probabilities nearly instantly once supplied with data and trained. This speed makes Bayesian networks an ideal tool for early warning systems, which require rapid decision making under uncertainty. Furthermore, they have the potential to lower barriers to entry for end users by presenting scientific output in a more accessible and interactive way.

The main disadvantage of Bayesian networks is that they are data-intensive, requiring sufficient input in order to derive the probabilistic relationships used in their predictions. This may make their application in data-poor environments (e.g., low-lying tropical islands) challenging. To overcome this limitation, we used a process-based numerical wave and water level model to generate a synthetic database of model results that captures a wide range of intrinsic coral reef properties and extrinsic hydrodynamic conditions. The network then acts as an emulator or surrogate for the process-based model, as also applied by Poelhekke et al. (2016). Given the numerous combinations of island morphologies and physical forcing, Bayesian networks are a powerful tool for improving our prediction strategies for wave-driven flooding threats.

This paper aims to demonstrate the use of a physics-based, deterministic numerical wave and water level model (XBeach Non-Hydrostatic) and probabilistic Bayesian network (Netica) for estimating wave-induced flooding of reef-fronted coastlines. First, the methodology used to construct the synthetic database and design the Bayesian network is reviewed, and then the results of the network, here termed, "Bayesian Estimator for Wave Attack in Reef Environments" (BEWARE), are presented and discussed. The findings focus on the most important parameters for estimating wave-driven flooding of reef-lined coasts, and the implications of using this system for early warning systems, climate change impact assessments, or adaptive planning such as prioritizing reef restoration projects. The resulting Bayesian estimator is powerful in that it will enable researchers and coastal managers to assess wave-induced flood hazards on a coast even if only approximate information is available. The paper is organized as follows. In section 2, we discuss the methods; in section 3, the results and analysis; in section 4, we discuss the implications of our findings and future applications; in section 5, we provide our conclusions. Additional material regarding the XBeach Non-Hydrostatic model validation, runup decomposition calculation, and BEWARE database are included in supporting information (S1).

2. Methods

To construct BEWARE, the results of a validated process-based numerical wave model were combined with a probabilistic Bayesian network. There are five steps in the methodology:

1. Schematize the reef and forcing conditions, and formulate a range of input parameters based on field measurements and typical values from the literature, as per Quataert et al. (2015).
2. Simulate nearshore hydrodynamics for the full range of parameters using the validated process-based wave and water level XBeach Non-Hydrostatic (XBHN) model to create a synthetic database of hydrodynamic responses to extrinsic forcing and intrinsic coral reef geomorphology.
3. Develop a Bayesian network and train with model results.
4. Validate the Bayesian network by comparing predictions to field observations.
5. Assess the performance of the Bayesian network using techniques such a log likelihood ratios and confusion matrices.

Table 1
Primary XBeach Non-Hydrostatic Model Input Parameters and Their Values

Parameter	Symbol	Units	Values
Offshore water level	η_0	m	$-1.0, -0.5, 0, 0.5, 1.0, 1.5, 2.0, 2.5, 3.0$
Offshore significant wave height	H_0	m	1, 2, 3, 4, 5
Offshore wave length	L_0	m	–
Offshore wave steepness	H_0/L_0	–	0.005, 0.001, 0.050
Fore reef slope	β_f	–	1/2, 1/10, 1/20
Reef flat width	W_{reef}	m	0, 50, 100, 150, 200, 250, 300, 350, 400, 500, 1,000, 1,500
Beach slope	β_b	–	1/5, 1/10, 1/20
Coefficient of friction	c_f	–	0.01, 0.05, 0.10

2.1. Model Reef and Forcing Schematization

Key parameters were chosen based on findings of previous studies, following the methodology outlined by Quataert et al. (2015). Multiple extrinsic and intrinsic parameters were covaried. The extrinsic hydrodynamic parameters were offshore water level (η_0), wave height (H_0), and wave steepness (H_0/L_0), while the intrinsic reef morphologic parameters examined were fore reef slope (β_f), reef flat width (W_{reef}), beach slope (β_b), and bed roughness (c_f), as shown in Figure 1. Values were chosen to represent typical conditions reported in the literature and observed at field sites (Table 1). Beach crest elevation, or island height (z_{beach}), was fixed at a height of 30 m to focus on runup as a proxy for overtopping, as per (Matias et al., 2012). However, the method can easily be extended to include lower values of z_{beach} for direct computation of overtopping.

2.2. Simulation of Nearshore Hydrodynamics

To generate the synthetic database, the process-based XBeach Non-Hydrostatic (XBNH) model (version 1.22.4867) was used with varying reef morphology and hydrodynamic forcing based on the schematization of section 2.1. XBNH is a depth-averaged, wave-resolving model that solves the shallow water equations including nonhydrostatic pressure (McCall et al., 2014; Smit et al., 2014; Roelvink et al., 2015). The model was first validated using data from a fringing reef hydrodynamics laboratory experiment (Demirbilek et al., 2007) (see supporting information S1).

An idealized 1-D reef profile was created in XBNH and varied for a range of parameter values (Table 1). This study extends the 57 XBNH simulations of Quataert et al. (2015) to 174,372 (seven parameters, 3–12 variations per parameter, and four 30 min simulation periods with random realizations of the surface elevation time series at the offshore boundary). A variable spin-up time was implemented to account for the differences in the time to achieve stationary conditions.

The XBNH model complexity had to be balanced carefully with time constraints because computational demand increases exponentially with the number of parameters and variations. The scope of this study was thus limited to remotely generated swell with unimodal JONSWAP spectra and maximum significant wave height of 5 m, rather than more extreme cyclone conditions. The idealized setup used here has several other limitations, in that it was one-dimensional, had spatially uniform bed roughness, and greatly simplified the complex bathymetry characteristic of most coral reefs. The application of a one-dimensional model along a cross-shore profile neglects some of the dynamics that occur on natural reefs, such as lateral flow. It does, however, represent a conservative estimate for IG wave generation and runup, as the forcing is shore-normal.

2.3. Development and Training of the Bayesian Network

Bayesian networks such as Netica (Norsys, 2003), which was used here, are probabilistic graphical models that rely on Bayesian probability to make predictions. By examining the statistical relationships between each result in the database, the network develops conditional probabilistic relationships between each parameter, which are updated as more data (here: model results) are added (see supporting information S2).

The first step in developing a Bayesian network is to define key parameters as nodes, and then to create links between them based on their dependencies. The eight main parameters varied in XBNH served as the input nodes. Output nodes or "hazard indicators" were chosen from model variables (Table 2) that either indicate the potential for flooding (in this case the top 2% of runup, $R_{2\%}$) or provide insight into the

Table 2
Primary XBeach Non-Hydrostatic Output Parameters, Calculated at the Inner Reef Flat Unless Otherwise Noted

Parameter	Symbol	Units
Significant sea/swell wave height (0.04–1 Hz)	$H_{m0,SS}$	m
Significant infragravity wave height (0.004–0.04 Hz)	$H_{m0,IG}$	m
Significant very low frequency wave height (0.001–0.004 Hz)	$H_{m0,VLF}$	m
Significant low-frequency wave height (0.001–0.04 Hz)	$H_{m0,LF}$	m
Wave setup	$\overline{\eta_{setup}}$	m
Mean water depth (averaged across entire reef flat)	h_{reef}	m
Extreme water level (mean of values greater than 2% exceedance value)	$\overline{\eta_{2\%}}$	m
Sea/swell contribution to $\overline{\eta_{2\%}}$ (0.04–1 Hz)	$\overline{\eta_{2\%,SS}}$	m
Infragravity contribution to $\overline{\eta_{2\%}}$ (0.004–0.04 Hz)	$\overline{\eta_{2\%,IG}}$	m
Very low frequency contribution to $\overline{\eta_{2\%}}$ (0.001–0.004 Hz)	$\overline{\eta_{2\%,VLF}}$	m
Runup (2% exceedance value) on beach slope	$R_{2\%}$	m
Runup (mean of values greater than 2% exceedance value)	$\overline{R_{2\%}}$	m
Sea/swell contribution to $\overline{R_{2\%}}$ (0.04–1 Hz)	$\overline{R_{2\%,SS}}$	m
Infragravity contribution to $\overline{R_{2\%}}$ (0.004–0.04 Hz)	$\overline{R_{2\%,IG}}$	m
Very low frequency contribution to $\overline{R_{2\%}}$ (0.001–0.004 Hz)	$\overline{R_{2\%,VLF}}$	m
Mean spectral period	$T_{m-1,0}$	s
Mean spectral frequency	$f_{m-1,0}$	Hz

hydrodynamic processes acting on reefs, such as mean wave period ($T_{m-1,0}$). The main Bayesian network configuration used here (Figure 2) assumes that all input parameters influenced each of the output parameters.

In order to represent the model variables as probability distributions, the data set was divided into bins (Figure 2). Input parameters were discretized using the same parameter values as were tested in XBNH, resulting in uniform distributions. Discretization of output variables required more careful consideration, since they were continuously distributed. Furthermore, because of nonlinear processes, a uniform input may yield a nonuniform output distribution, which influences bin discretization. The chosen bins took into account both the distribution of data and the desired precision of the estimates. Care was taken to prevent overfitting by checking that increasing the number of bins per node did not increase validation error rates, as per Gutierrez et al. (2015). The last step in constructing the Bayesian network was to train it using the synthetic data set created with XBNH, resulting in the prior predictions (i.e., probability distributions of all model results in the absence of additional information or constraints). Simulations that did not achieve stationary conditions before the end of the spin-up period (30–120 min, depending on reef width) were excluded from the Bayesian network.

2.4. Bayesian Network Validation

The Bayesian network was constructed using a synthetic data set, so it needed to be validated using field data from case studies. However, there are limited suitable field measurements available, so at this time only a field data set from Roi-Namur in the Republic of the Marshall Islands (Quataert et al., 2015; Cheriton et al., 2016; Gawehn et al., 2016) and numerical model results from Funafuti, Tuvalu (Beetham et al., 2015), were used for validation. The availability of additional runup time series recorded on fringing coral reef-fronted beaches would provide more opportunities to test the network, although this is hampered by the dearth of published $R_{2\%}$ field measurements in such locations.

To test the network, input nodes were constrained based on the prescribed hydrodynamic boundary conditions and given reef geomorphology. The posterior probability distributions of runup, wave height at the toe of the beach (SS, IG, and VLF frequencies), and wave setup were then compared with their observed values. An ideal prediction would show a narrower posterior distribution (indicative of precision) that is centered on the observed value (representative of accuracy).

2.5. Assessment of Bayesian Network Performance

The performance of the Bayesian network (how often estimates are correct) was assessed by comparing the predictive skill of different configurations, and by testing its accuracy in predicting a subset of the database
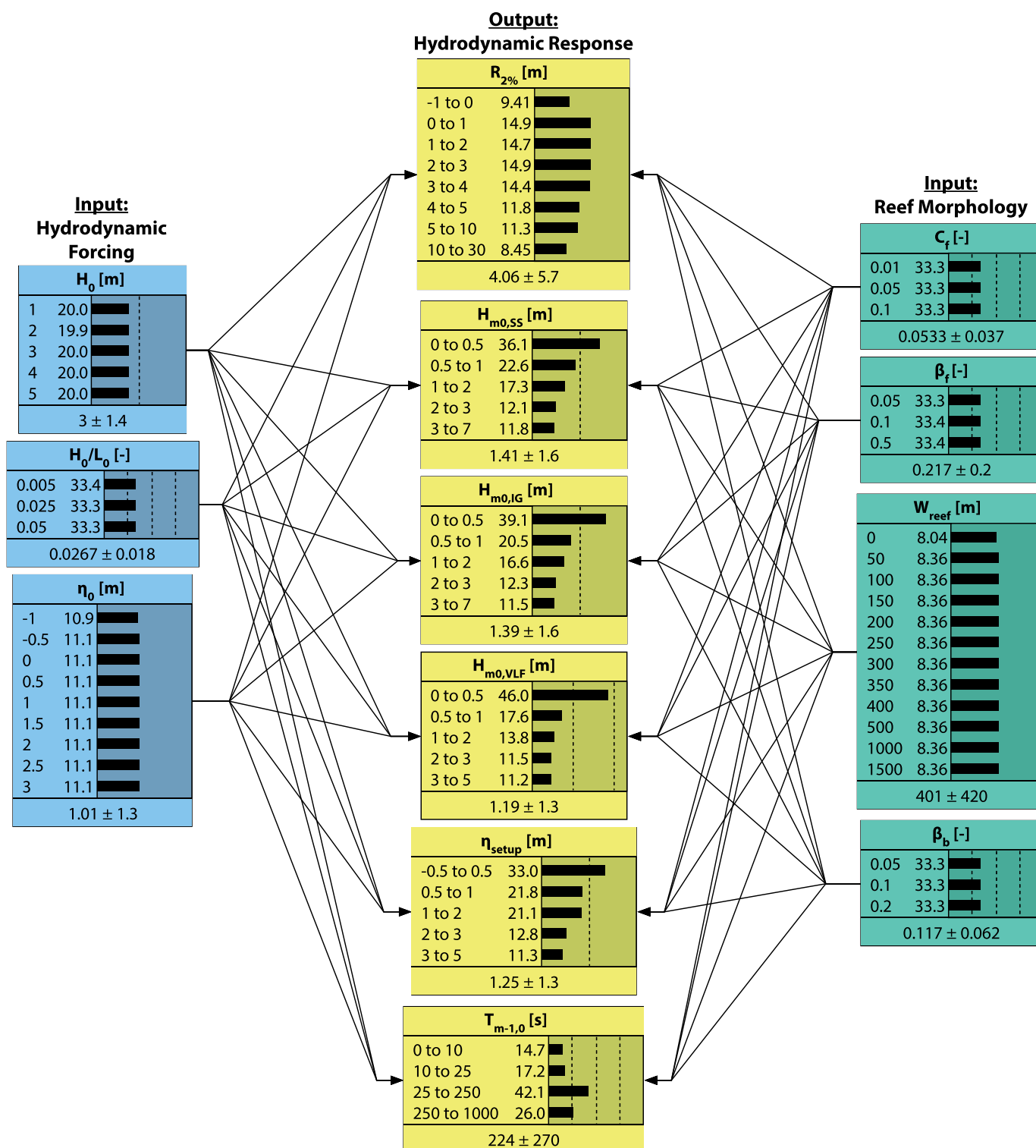
Figure 2. Layout of the "Bayesian Estimator for Wave Attack in Reef Environments" (BEWARE) system, illustrating key parameters and the links between them. Extrinsic hydrodynamic input parameters are shaded in blue, intrinsic reef morphologic input parameters in teal, and output variables (calculated at the inner reef flat/beach toe) in yellow. Within the nodes are a histogram indicating the prior probability distributions, mean, and standard deviation for each parameter ($n = 174{,}372$). The key parameters are defined in Tables 1 and 2. Negative values of $R_{2\%}$ can be explained by cases where $\eta_0 < 0$ and runup on the fore reef does not exceed the reef crest. Negative values of η_{setup} can be explained by cases where the $W_{reef} = 0$ and set down is occurring at the observation point.

that had been excluded from the training. The first means of evaluating the predictive skill of the Bayesian network here was through the use of confusion matrices, which break down predictive error rates into over-prediction and underprediction. A confusion matrix thus provides a "hit rate" for the Bayesian network, identifying how often the network correctly predicts what was observed in reality, or, in this case, calculated by the XBNH model. To compute the error rates and confusion matrices, a k-fold cross validation was performed, as per Poelhekke et al. (2016) and Gutierrez et al. (2015). This entailed randomly dividing the database into k (in this case 10) folds or subsets, excluding them one at a time from the training, and comparing the network predictions of the excluded data with the actual values. Although there is no restriction on the size of confusion matrices, their complexity increases greatly with the number of bins for a given output node. Hence, only a binary confusion matrix (two bins) was considered here, such that a variable lying below a set threshold was considered negative, and positive above the threshold.

The second method for assessing the predictive capability of the network was using the log likelihood ratio (LLR). The LLR is an indicator of predictive skill and model uncertainty that compares the prior predictions of a network with the posterior predictions made using additional information (Plant & Holland, 2011). The concept is explained in more detail by, van Verseveld et al. (2015), Gutierrez et al (2015), and Poelhekke et al. (2016). When the LLR is calculated for key parameters, it makes it possible to consider which parameters should be included in the Bayesian network, which parameter uncertainty should be constrained, and, thus, which field measurements are most important to collect. By withholding parameters from the network one at a time and comparing the resulting predictions with those of the full network, the relative importance of each parameter was assessed. For this study, the LLR score for each withheld parameter was normalized by the LLR score of the full network.

3. Results and Analysis

3.1. XBNH Validation on Reefs

In order to validate XBNH and the parameter settings for wave transformation and runup on a fringing reef, the model was tested against the Demirbilek et al. (2007) laboratory-derived experimental data set of cases without wind, similar to the data sets used by Nwogu & Demirbilek (2010), Zijlema (2012), and Shimozono et al. (2015) to validate their numerical models.

Modeled H_{m0} at the inner reef flat shows good agreement with the laboratory data across the 29 tested cases (Figure 3a), albeit with slight underestimation ($R^2 = 0.786$, bias $= -0.098$). The model shows greater skill at estimating wave setup at the inner reef flat, also with a slight negative bias ($R^2 = 0.946$, bias $= -0.046$), as shown in Figure 3b. The scatter in $R_{2\%}$ predictions is wider but shows a positive correlation and slight overestimation ($R^2 = 0.642$, bias $= +0.098$), as shown in Figure 3c. The results of this validation suggest that XBNH can simulate reef hydrodynamics with reasonable accuracy, and give us the
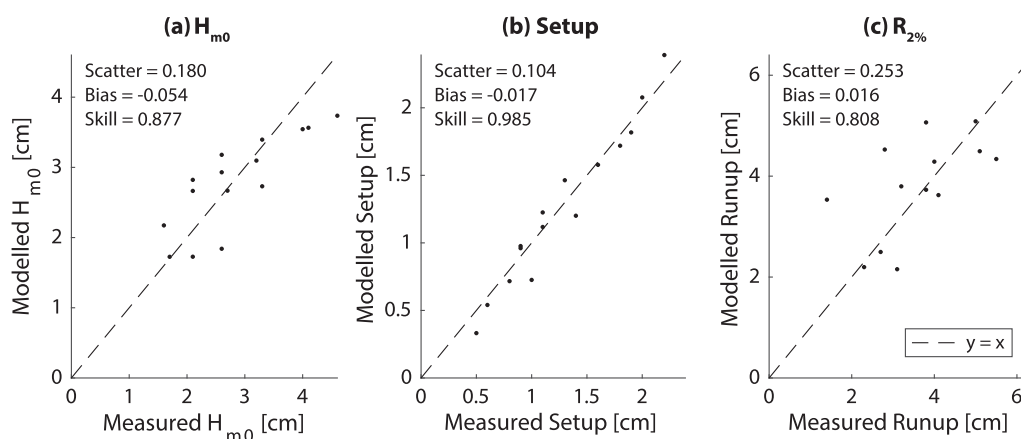
Figure 3. Scatterplots of observed (Demirbilek et al., 2007) and computed properties at the inner reef flat (a) wave height (H_{m0}), (b) setup, and (c) runup ($R_{2\%}$) for all 15 tested cases.

confidence to use it in the subsequent analysis. More information regarding the validation can be found in supporting information (S1).

3.2. XBNH Results

The nearshore hydrodynamic results of all XBNH simulations were aggregated to enable an examination of general trends across the entire synthetic data set (Figure 4). Extreme water levels on the inner reef flat ($\overline{\eta_{2\%}}$) and runup ($\overline{R_{2\%}}$) were defined as the mean of the highest 2% of the water level time series for each simulation at the inner reef flat and waterline, respectively. We focus on η at the inner reef flat because it is commonly measured in reef hydrodynamics studies (i.e., Cheriton et al., 2016; Merrifield et al., 2014), and on $R_{2\%}$ because it can be used as a proxy for overtopping and potential flooding (Matias et al., 2012). These
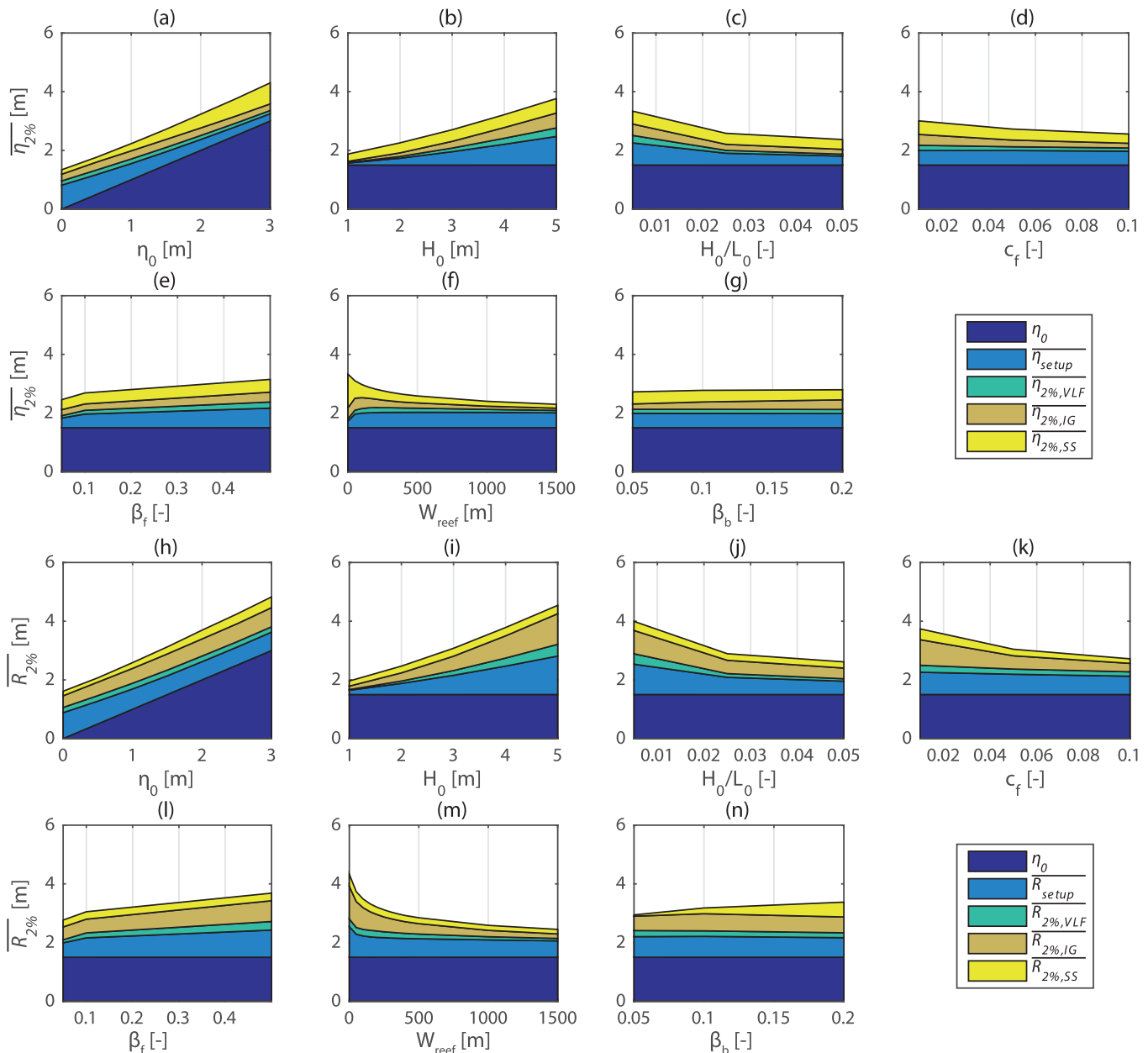

Figure 4. For the full set of XBeach Non-Hydrostatic simulations, variations in (a–g) extreme water levels, $\overline{\eta_{2\%}}$, and (h–n) runup, $\overline{R_{2\%}}$, as a function of the seven primary input parameters (Table 1). The different colors represent the mean relative contribution of water level (η_0), setup, and each wave frequency band (VLF, very low frequency, 0.004–0.001 Hz; IG, infragravity, 0.04–0.004 Hz; SS, sea swell, >0.04 Hz) to the total water level and runup. Results have been filtered to show only cases with $\eta_0 \geq 0$ ($n = 136,032$).
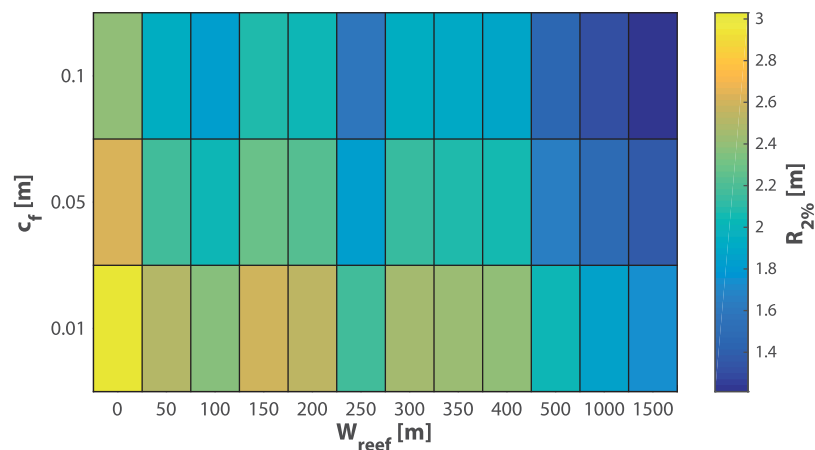
Figure 5. Runup ($R_{2\%}$) as a function of reef width (W_{reef}) and friction coefficient (c_f), averaged across all tested XBeach cases ($n = 174,372$).

values were then decomposed into separate components (i.e., η_0, $\overline{\eta_{setup}}$, $\overline{\eta_{2\%,SS}}$, $\overline{\eta_{2\%,IG}}$, $\overline{\eta_{2\%,VLF}}$) to yield insight into the nature of wave transformation across the reef. This decomposition calculation is described in supporting information (S3).

Some trends confirm a priori expectations: the extreme water level parameters $\overline{\eta_{2\%}}$ and $\overline{R_{2\%}}$ both increase with increasing η_0 and H_0 (Figures 4a, 4b, 4h, and 4i), and both decrease for high H_0/L_0 (Figures 4c and 4j). In addition, the highest extreme water levels occur with low c_f (Figures 4d and 4k), small W_{reef} (Figures 4f and 4m), steep β_f (Figures 4e and 4l), and steep β_b (Figures 4g and 4n), which concurs with the findings of Quataert et al. (2015) and Shimozono et al. (2015). When runup ($R_{2\%}$) is evaluated as a function of reef width and friction (Figure 5), it increases with reduced width (consistent with Shimozono et al., 2015) and reduced friction (consistent with Quataert et al., 2015).

For a constant water level, as offshore wave heights increase, extreme water levels and runup at the shoreline become primarily driven by setup and reef flat waves. With increasing H_0, the combined contribution of $\overline{\eta_{setup}}$, $\eta_{2\%,SS}$, $\eta_{2\%,IG}$, and $\overline{\eta_{2\%,VLF}}$ (i.e., excluding η_0) to total $\overline{\eta_{2\%}}$ increases from 20% to 60% (Figure 4b), and similarly, the contribution of R_{setup}, $R_{2\%,SS}$, $\overline{R_{2\%,IG}}$, and $\overline{R_{2\%,VLF}}$ to total runup ($\overline{R_{2\%}}$) rises from 23% to 67% (Figure 4i). The large contribution of setup and reef flat waves to total extreme shoreline water levels and runup during the occurrence of large offshore waves reinforces the importance of including these parameters in predictions of flooding on reef-lined coasts, as opposed to simpler "bathtub" models that only account for offshore water levels. Variations in H_0/L_0 (Figures 4c and 4j) and β_f (Figures 4e and 4l) have little effect on the relative composition of $\overline{\eta_{2\%}}$ and $\overline{R_{2\%}}$, but there is a proportionally larger $\overline{R_{2\%,IG}}$ component at lower values of c_f (23% of $\overline{R_{2\%}}$ at $c_f = 0.01$, up from 11% at $c_f = 0.1$; Figure 4k), indicating the importance of frictional dissipation to resulting infragravity wave dynamics over reef flats. This relationship has been indicated by field data (Cheriton et al., 2016) and physics-based models (Pomeroy et al., 2012a), particularly in relation to resonance.

While offshore wave forcing is important, mean offshore water level (η_0) was found to have the strongest effect on the relative proportions of setup and reef flat waves to overall extreme shoreline water levels and runup. Wave-driven setup makes up the largest proportion of $\overline{\eta_{2\%}}$ at lower values of η_0 (61% at 0 m; Figure 4a), but its influence decreases with increasing water depth on the reef flat (6% at 3 m); this inverse relationship between water level setup and offshore water levels is well established (Becker et al., 2014; Beetham et al., 2015; Vetter et al., 2010). Infragravity and VLF waves make a fairly constant contribution across the full range of modeled water levels ($\overline{\eta_{2\%,IG}}$: $\mu = 0.14$ m, $\sigma = 0.02$ m; $\overline{\eta_{2\%,VLF}}$: $\mu = 0.25$ m, $\sigma = 0.02$ m); this relative insensitivity of low-frequency waves to offshore water level was also observed in the field (Beetham et al., 2015; Merrifield et al., 2014). However, for the short-period waves, since they are depth-limited, as the mean water level over the reef flat increases, the contribution of $\overline{\eta_{2\%,SS}}$ to the total $\overline{\eta_{2\%}}$ increases (from 0.15 m [11%] at 0 to 0.72 m [17%] at 3 m). However, while the magnitude of the contribution of SS waves to runup, $\overline{R_{2\%,SS}}$, increases with increasing η_0, the relative proportion does not (from 0.16 m [10%] at 0 to
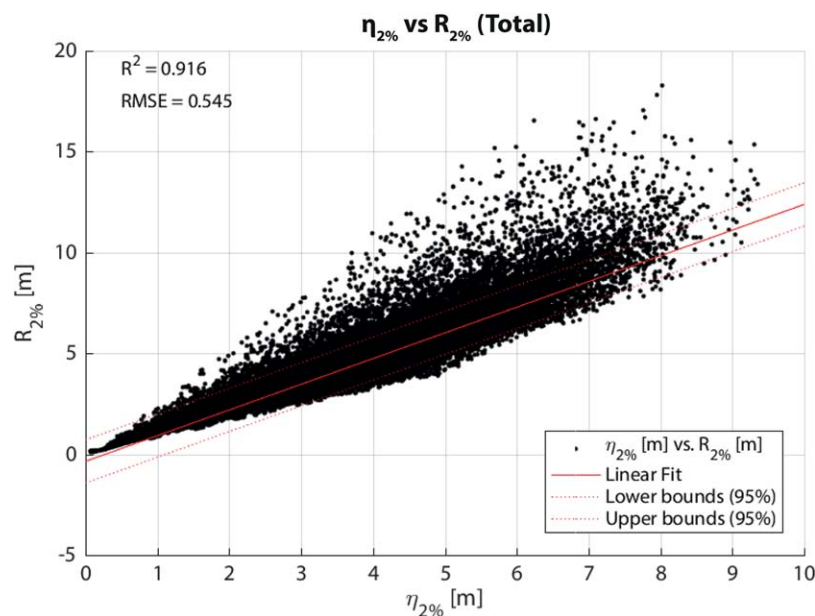
Figure 6. Extreme water levels at the inner reef flat ($\overline{\eta_{2\%}}$) versus runup on the beach slope ($\overline{R_{2\%}}$). Results have been filtered to show only cases with $\eta_0 \geq 0$ and $z_{beach} = 30$ m ($n = 136{,}032$).

0.36 m [8%] at 3 m). This modulation of SS waves by offshore water level is consistent with previous findings (Beetham et al., 2015; Merrifield et al., 2014; Storlazzi et al., 2011). Because increases in η_0 can be considered a proxy for sea level rise, these findings imply that sea level rise may result in a greater contribution to extreme shoreline water levels and runup from SS-band reef flat waves.

Although the composition of $\overline{\eta_{2\%}}$ is relatively insensitive to different beach slopes, β_b, (Figure 4g), $\overline{R_{2\%}}$ shows some variation (Figure 4n), with the contribution of $\overline{R_{2\%,SS}}$ increasing with steeper β_b (from 2% to 15% of total). This trend was also noted by Shimozono et al. (2015), as runup is inversely proportional to dissipation in the surf zone. Furthermore, higher-frequency waves break more readily on milder beach slopes where they are depth limited (Brocchini & Baldock, 2008).

The overall trends for $\overline{\eta_{2\%}}$ and $\overline{R_{2\%}}$ are similar, although $\overline{R_{2\%}}$ is consistently ~27% higher than $\overline{\eta_{2\%}}$ for the same forcing conditions (Figure 6). This may have important implications for inferring $\overline{R_{2\%}}$ and flooding characteristics from measurements on the reef flat in the absence of direct $\overline{R_{2\%}}$ measurements. Although directly correlated ($R^2 = 0.916$), $\overline{\eta_{2\%}}$ by itself does not fully translate to $\overline{R_{2\%}}$, as a result of continued wave transformation on the beach slope.

In this section, we examined the average of all conditions in the data set, but there is considerable variation around the mean. These variations can be attributed, in part, to particular combinations of parameters that yield anomalously high runup, such as those that result in resonant amplification, which is explored in the next section.

3.3. Reef Flat Resonance

As reef flat resonance may account for anomalously high runup (Gawehn et al., 2016; Nakaza et al., 1990; Nwogu & Demirbilek, 2010; Shimozono et al., 2015), the model results were analyzed to determine if resonant conditions were present. A peak in $H_{m0,VLF}$ wave height at the inner reef flat was identified for narrower (~50 to 250 m) reefs (Figure 7a). In order to verify whether this peak was related to resonance, cases of relatively high (top 30%) IG and VLF waves, defined as $\left(H_{m0,IG}/H_0\right)^2 > 0.3$ and $\left(H_{m0,VLF}/H_0\right)^2 > 0.1$, respectively, were isolated for additional analyses. The data from these cases reveal a distinct peak (Figure 7b) at the resonant frequency ($f_{m-1}/f_{n0} = 1 \pm 0.1$), indicating that resonance is likely occurring. Frictional and geometrical effects can explain deviations from the theoretical resonant frequency (van Rijn, 2011). Furthermore, not all high-energy VLF waves are necessarily resonant: some may also be standing or progressive waves (Gawehn et al., 2016).
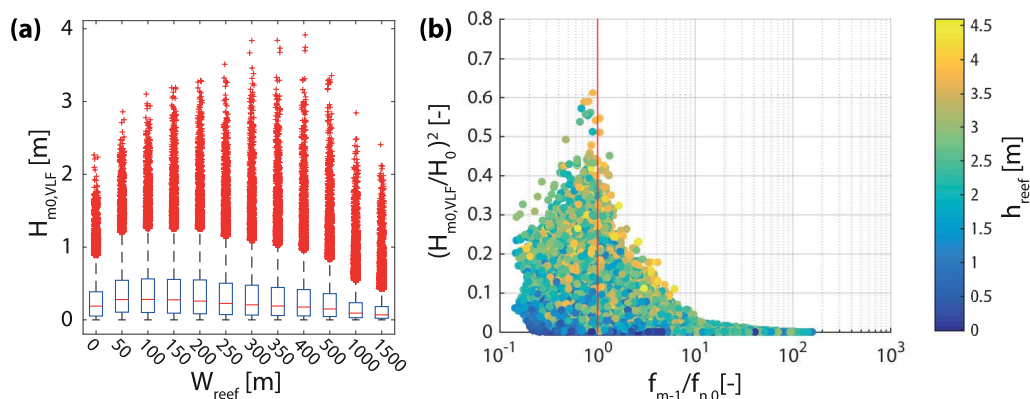
Figure 7. (a) VLF wave height as a function of reef width ($n = 174{,}372$). The red line indicates the mean, blue box indicates 25th and 75th percentiles, and black whiskers denote the 5th and 95th percentiles, with red dots indicating upper-range outliers. (b) Normalized, squared VLF wave height ($H_{m0,VLF}/H_0)^2$ as a function of the ratio between mean spectral frequency at the inner reef flat ($f_{m-1,0}$) and the reef's zeroth resonant frequency ($f_{n,0}$). Points close to $f_{m-1,0}/f_{n,0} = 1$ ($10°$) are near resonance.

To quantify the differences between mean conditions and resonant cases, the full set of model results was filtered, selecting only those cases meeting the aforementioned resonance criteria, and the same analyses of comparing the contributions to extreme shoreline water levels and runup were carried out for only these resonance cases (Figure 8). In general, $\overline{\eta_{2\%}}$ and $\overline{R_{2\%}}$ were slightly higher for the resonant cases in Figure 8 when compared to the full set of simulations shown in Figure 4. The starkest difference between the resonance-only and full set of simulations is found with the $\overline{\eta_{2\%}}$ and $\overline{R_{2\%}}$ trends as a function of reef width: as W_{reef} increases, $\overline{\eta_{2\%}}$ and $\overline{R_{2\%}}$ values from the full set of model results gradually decline (Figures 4f and 4m), while the $\overline{\eta_{2\%}}$ and $\overline{R_{2\%}}$ values for the resonance cases increase sharply (Figures 8f and 8m). The discontinuity at 500 m is due to the fact that none of the simulations with $W_{reef} > 500$ m met the aforementioned resonance criteria. Furthermore, the percent contribution of $\overline{\eta_{2\%,IG}}$ to $\overline{\eta_{2\%}}$ is larger than that of $\overline{\eta_{2\%,VLF}}$ for $W_{reef} < 300$ m, whereas the percent contribution of $\overline{\eta_{2\%,VLF}}$ to $\overline{\eta_{2\%}}$ is larger at $W_{reef} > 300$ m (Figure 8f), likely due to resonance. When theoretical resonant frequencies are calculated for a mean reef flat depth (h_{reef}) of approximately 1.5 m across all simulations using Equation (1), $W_{reef} < 240$ m should be resonant at IG frequencies, and resonant at VLF frequencies when $W_{reef} > 240$ m. A similar shift from IG to VLF energy on wider reefs was also demonstrated by Shimozono et al. (2015).

Many of these resonant cases are associated with greater mean reef flat water depths (h_{reef}), whether due to higher η_0 or setup (Figure 8a). This coincides with the expected response, since greater water depth over the reef increases the resonant frequency and reduces the effects of frictional dissipation (Péquignet et al., 2009; Pomeroy et al., 2012a). Shimozono et al. (2015) also posited that the increase from extreme water levels at the inner reef flat to runup on the shoreline can be partly attributed to resonant runup amplification along the beach slope. However, this effect was found to be minor for the steep range of β_b tested here. The trends in percent contribution of setup and the different wave frequency components to total extreme water levels and runup are relatively similar between the resonant cases (Figure 8) and the full set of simulations (Figure 4).

Though large $\overline{R_{2\%,VLF}}$ values are seen for $W_{reef} \sim 250$–500 m in resonance cases (Figure 8m), a similar increase in runup as a function of reef width is not seen for the full suite of cases (Figure 4m) because resonant cases are rare ($n = 7{,}608$) relative to all others in the data set ($n = 136{,}032$). However, given that the synthetic data set is based on uniform input distributions, and T_p values that are a function of H_0 (via the steepness parameter), it is possible that resonant cases are underrepresented here compared to what might be expected in the field.

3.4. Bayesian Network Validation
In the next step, the Bayesian network was trained using the results from XBNH, and validated against field data from the 18 November 2013 runup event on Roi-Namur in the Republic of the Marshall Islands (Cheriton et al., 2016; Quataert et al., 2015), and model simulations of the 23 June 2013 runup event on Funafuti,
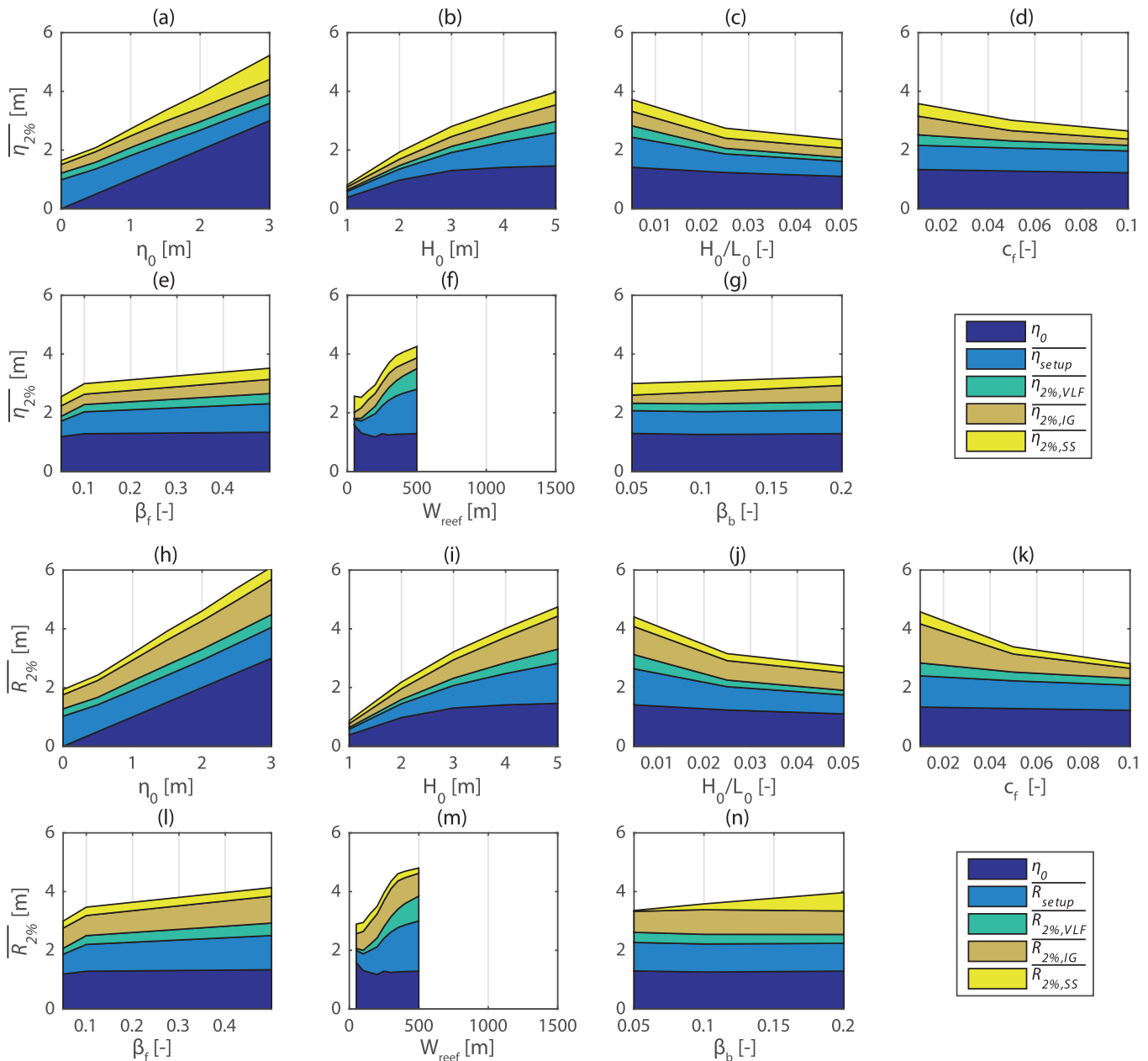
Figure 8. For the XBeach Non-Hydrostatic (XBNH) model resonance cases, variations in (a–g) extreme water level, $\overline{\eta_{2\%}}$, and (h–n) runup, $\overline{R_{2\%}}$, as a function of the seven primary input parameters (Table 1). The different colors represent the mean relative contribution of water level (η_0), setup, and each wave frequency band (VLF, very low frequency, 0.004–0.001 Hz; IG, infragravity, 0.04–0.004 Hz; SS, sea swell, >0.04 Hz) to the total water level. Resonant cases were filtered from the full set of XBNH simulations presented in Figure 4 by selecting only simulations where $f_{m-1,0}/f_{n,0} = 1 \pm 0.1$ ($n = 7,608$).

Tuvalu (Beetham et al., 2015). The prior distributions in Figure 2 (also presented in Figure 9 in a different format) indicate the default prediction for each hazard indicator without any additional information (dark blue bars in Figure 9). When the observed hydrodynamic forcing and reef characteristics are introduced to the Bayesian network, the hazard predictions are constrained, yielding the posterior distributions. The network's predictive skill is judged based on whether the peak of the posterior prediction matches the observed value for each hazard variable. In the Funafuti cases, results are presented as maximum runup (R_{max}) and contributions to R_{max} ($R_{max,SS}$ and $R_{max,LF}$), so we used $\overline{R_{2\%}}$, $\overline{R_{2\%,SS}}$, and $\overline{R_{2\%,LF}}$ to make comparisons rather than $R_{2\%}$, $H_{m0,SS}$, and $H_{m0,LF}$ as with Roi Namur.
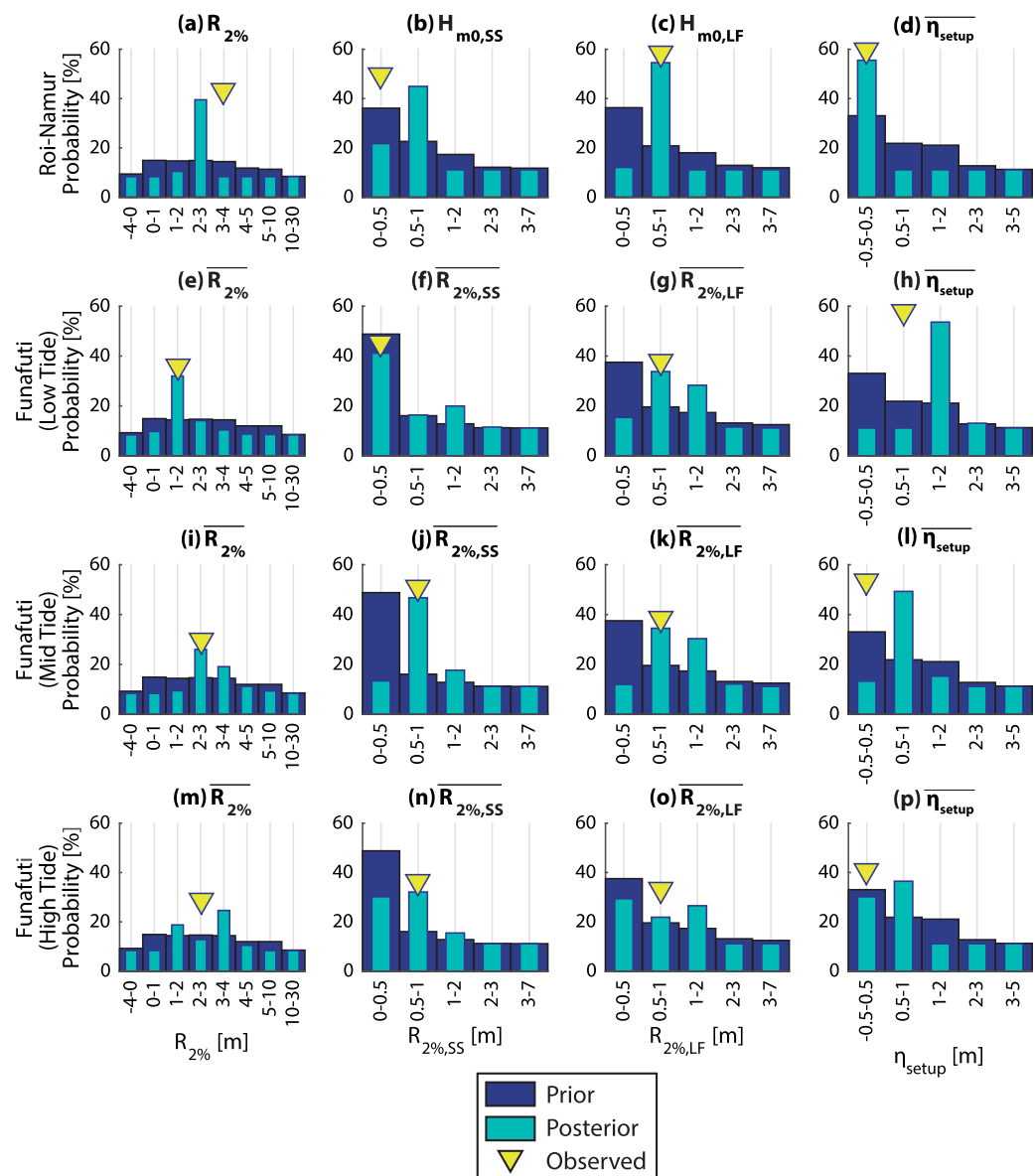
Figure 9. The "Bayesian Estimator for Wave Attack in Reef Environments" (BEWARE) system validation against case studies. Figures 9a–9d correspond to the runup event on 18 November 2013 in Roi Namur, Republic of the Marshall Islands (Cheriton et al., 2016; Quataert et al., 2015). Figures 9e–9p correspond to a runup event on Funafuti, Tuvalu modeled by Beetham et al. (2015). Please see Table 2 for parameter definitions. Note that for these test cases, $H_{m0,LF}$ and $\overline{R_{2\%,LF}}$ encompass the full range of low-frequency waves from 0.001 to 0.04 Hz (i.e., including infragravity waves), as per the convention used in the data sources. The dark blue bars represent the prior probability distribution for all cases in the network, and the lighter blue bars represent the posterior probability distributions, based on the hydrodynamic forcing and reef characteristics of each test case. The yellow triangles indicate the observed values of each variable from the case study.

The network underestimates $R_{2\%}$ for Roi-Namur (Figure 9a), and overestimates $\overline{R_{2\%}}$ for the Funafuti high tide case (Figure 9m), albeit by a single bin (20 cm elevation difference). However, it correctly predicts runup for the low and mid tide Funafuti cases (Figures 9e and 9i). Although the network overpredicts $H_{m0,SS}$ ($f > 0.04$ Hz) on Roi-Namur (Figure 9b), it successfully estimates $\overline{R_{2\%,SS}}$ for the Funafuti cases (Figures 8f, 8j, and 8n). $H_{m0,LF}$ and $\overline{R_{2\%,LF}}$ ($f < 0.04$ Hz) are confidently and correctly predicted by the network in three of the tested cases (Figures 9c, 9g, and 9k), although the bimodal posterior probability distribution for Funafuti at high tide (Figure 9o) suggests lower confidence in that prediction. Setup is overestimated for the Funafuti cases (Figures 9h, 9l, and 9p) but correctly predicted for Roi-Namur and Funafuti at high tide (Figure 9d).

Table 3

Confusion Matrices Depicting the Accuracy of the Bayesian Network in Predicting the XBeach Non-Hydrostatic (XBNH) Model Output Parameters (Table 2) for a Given Set of Input Conditions (i.e., Validation Error Rates)

Legend

Variable	Observed	Predicted Low	Predicted High
	Low	True Negative	False Positive
	High	**False Negative**	**True Positive**

(a) $R_{2\%}$ (m)

Observed	0 to 2	2 to 30
0 to 2	93.0	7.0
2 to 30	1.2	98.8

(b) η_{setup} (m)

Observed	0 to 1	1 to 5
0 to 1	98.4	1.6
1 to 5	2.1	97.9

(c) $T_{m-1,0}$ (s)

Observed	0 to 25	25 to 1000
0 to 25	93.9	6.1
25 to 1000	1.0	99.0

(d) $H_{m0,SS}$ (m)

Observed	0 to 1	1 to 7
0 to 1	99.5	0.5
1 to 7	2.6	97.4

(e) $H_{m0,IG}$ (m)

Observed	0 to 0.5	0.5 to 7
0 to 0.5	98.0	2.0
0.5 to 7	3.5	96.5

(f) $H_{m0,VLF}$ (m)

Observed	0 to 0.5	0.5 to 5
0 to 0.5	96.9	3.1
0.5 to 5	15.1	84.9

Note. Values in the tables indicate the percentage of observed cases falling into a given prediction bin. Green values along the main diagonal indicate correct predictions, whereas the bottom left corner indicates the false negative rate (underpredictions) and the top left indicates the false positive rate (overpredictions).

These results suggest that the Bayesian network is capable of predicting wave transformation processes across the reef for the majority of the limited cases that were accessible, but that it is less able to capture the final transformation from the inner reef flat across the beach. Discrepancies could be explained in part by the schematized nature of the XBNH model when compared to the real conditions of the reefs, or to differences in the runup/wave height decomposition calculation used by the validation cases. Underestimation of the Roi-Namur case may also be explained by the available measurements—the observed runup value is a single wave event that was captured on camera and may not correspond well with a statistical value like $R_{2\%}$. The limited published data available for validation of flooding hazards on reefs underscores the great need for further field measurements.

3.5. Bayesian Network Predictive Skill

After validating the Bayesian network on field and model data, its prediction of the XBNH results was tested, making it possible to draw on a much larger pool of data for comparison. This provides some insight into how often the Bayesian network overpredict or underpredict certain hazard indicators. The confusion matrices in Table 3 indicate that the network has high positive prediction rates for large values of $R_{2\%}$, η_{setup}, $T_{m-1,0}$, $H_{m0,SS}$, and $H_{m0,IG}$ (>96% correct) but is slightly less skilled at predicting large $H_{m0,VLF}$ (~85%). The high predictive skill for most of the hazard indicators (particularly runup) suggests that the Bayesian network acts here as a suitable proxy for XBNH, similarly to the findings of Poelhekke et al. (2016) for the XBeach Surf Beat model.

3.6. Bayesian Network Log Likelihood Ratio

After establishing the validity and performance of the network, the LLR test was used to investigate the relative importance of each parameter within the Bayesian network. When the normalized LLR was calculated for $R_{2\%}$ by withholding each input parameter successively from the network, it scored much lower when H_0, η_0, and W_{reef} were not taken into account (Figure 10a). This indicates that those parameters are more important for making successful predictions of runup (and by extension flooding) than parameters such as H_0/L_0, c_f, β_f, or β_b. Compared to the runup, setup is less sensitive to c_f (Figure 10b), as the setup is dominated by a balance between the radiation stress gradients and the pressure gradient with the friction force being a smaller component. The $T_{m-1,0}$ (Figure 10c) is sensitive mostly to W_{reef} and η_0 as these parameters control the degree to which the energy shifts to lower frequencies. $H_{m0,SS}$ (Figure 10d) shows similar behavior as the runup. Compared to the short waves, $H_{m0,IG}$ (Figure 10e) is less dependent on η_0 because it is not saturated and more determined by the breakpoint-generation and frictional dissipation processes as evidenced the sensitivity to H_0, H_0/L_0 and c_f. $H_{m0,VLF}$ (Figure 10f) shows poor predictive skill without H_0, H_0/L_0, β_f, and W_{reef}, indicating both offshore forcing and geometry are important to this response. This may reflect the highly nonlinear nature of processes controlling $H_{m0,VLF}$ (i.e., resonance), and may also explain the lower predictive accuracy observed for this variable in Table 3.
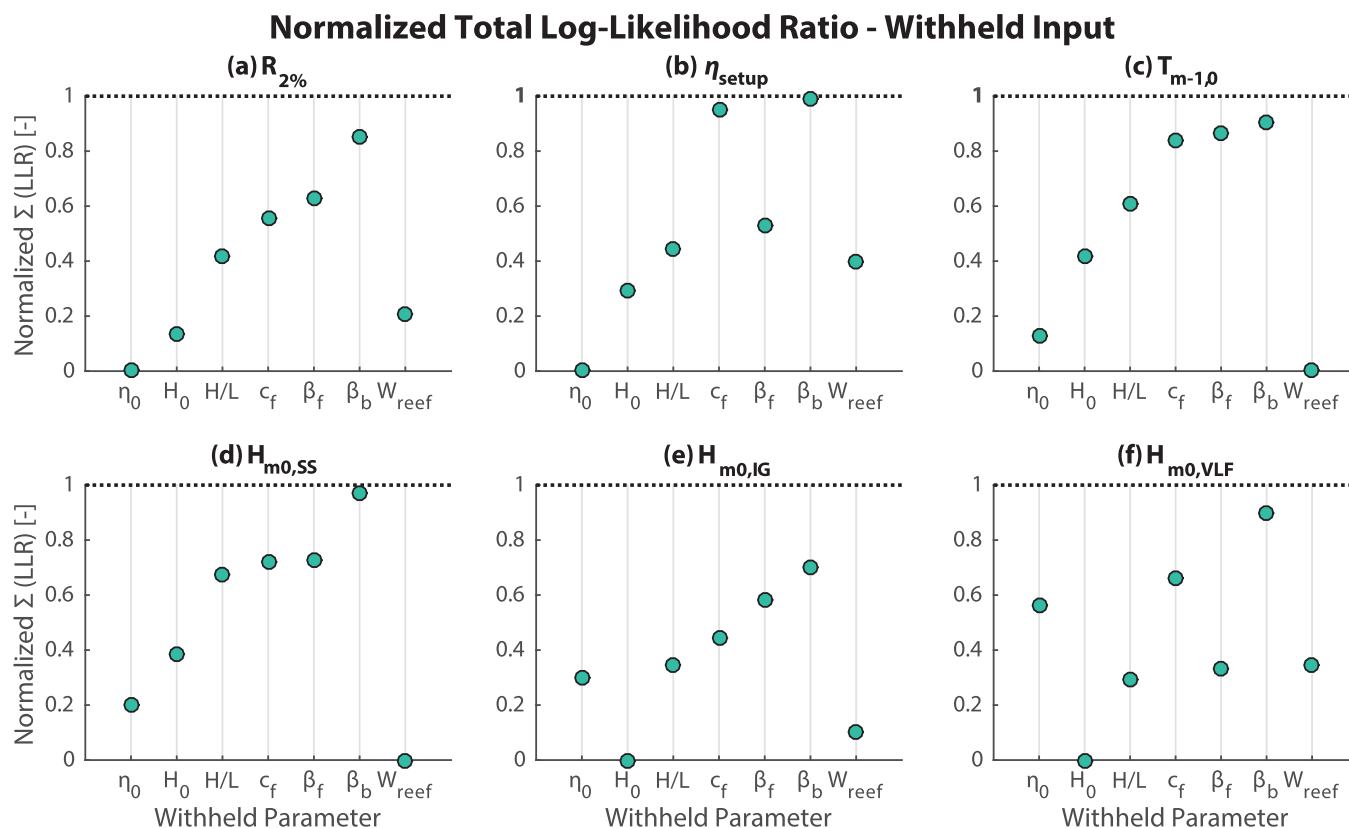
Normalized Total Log-Likelihood Ratio - Withheld Input

Figure 10. Log likelihood ratio (LLR) comparisons of key output variables (Table 2) for withheld parameters. The dashed line at y = 1 shows the normalized total LLR for the full network with all parameters included. Each of the circles represents the total LLR for a network where that parameter has been withheld from the prediction, normalized by the total LLR for the full network. A value of 1 would indicate that removing a given parameter does not affect the network's predictive skill, whereas a value of 0 means that the parameter is essential to making predictions of a particular output variable.

4. Discussion

This study presents a proof-of-concept for the use of a process-based model and Bayesian network to estimate flood hazard indicators such as runup on low-lying coral reef-lined coasts. This section examines the sensitivity of key parameters and potential future applications in early warning systems and climate change impact assessments.

4.1. Relevance of Key Parameters

The results of the LLR tests (Figure 10) across the entire data set indicate that hydrodynamic forcing (e.g., H_0, η_0, and H_0/L_0) is most important to an accurate prediction of the hydrodynamic response on the reef, followed by morphological characteristics. Of these, reef geometry parameters (e.g., β_f and W_{reef}) are more influential than the frictional characteristics (c_f) and beach slope β_b. The LLR tests imply that reef properties that can be more easily obtained via remote sensing (e.g., W_{reef} and β_f) may provide (to first order) more useful information than detailed, labor-intensive field surveys to measure parameters such as bed roughness (c_f). Similarly, although measurements of beach slope β_b are unavailable for most low-lying tropical islands, the LLR tests suggest that it is not critical for effective prediction of flooding hazards.

4.2. Bayesian Network Improvements

The network's validation could be improved by training it with additional XBNH simulations that include higher resolution of input parameters (e.g., $H_0 = 0.5, 1.5, 2.5, 3.5, 4.5$ m). Furthermore, the predictive skill of a Bayesian network improves when it has multiple cases from which to learn and gain experience (*Poelhekke et al.*, 2016). At present, four cases were simulated with random wave forcing for each combination of input parameters; the network's experience could be improved by increasing this number. Lastly, the

discretization of the Bayesian network's output bins directly influences the accuracy and precision of its predictions, so sensitivity to alternate configurations could be carried out. For instance, if the observed value was 0.51 and the predicted bin was 0.00–0.50, it would still be regarded as an incorrect prediction, even though it was very close.

4.3. Early Warning Systems

The Bayesian network presented in this study can be used in an early warning system (EWS) to predict flooding. Currently, most operational EWSs are capable of predicting offshore wave heights, tides and surges, but not onshore hazards such as runup and flooding because these are computationally expensive to predict. Following Poelhekke et al. (2016), one solution is to precompute the range of offshore forcing and onshore hazards, compile the results in a Bayesian network, and then couple this network to an EWS. Predictions of offshore forcing can be then used to obtain constrained posterior probability distributions of the onshore hazard at negligible computational expense in operational mode. The alternative method of incorporating a wave transformation model such as XBNH directly into an EWS (as was done in Bosserelle et al., 2015) does not have these advantages of speed and capability to quantify the hazard uncertainty.

In the case of an EWS for low-elevation, reef-lined islands, the offshore forcing can be obtained as follows: tides can be computed from a deterministic prediction, surges may be predicted using a hydrodynamic model such as Delft3D (although they are usually less important on steep-sloped coasts like atolls), and offshore wave predictions can be obtained from existing operational models such as WAVEWATCH-III (Tolman, 2009).

If coupled with 2-D inundation models, the EWS can be extended to predict flooding occurrence, timing and extent, which can be used for land use planning and evacuation purposes. Furthermore, if building characteristics are known, damage to structures could also be estimated using simple stage-damage relationships or more sophisticated approaches where sufficient data is available. van Verseveld et al. (2015) and Jäger et al. (2015, 2017) have used Bayesian networks to predict direct economic damage to houses and infrastructure resulting from surge and wave-induced flooding on sandy, urbanized coastlines.

4.4. Climate Change Impact Assessments

In addition to EWS, the BEWARE system can be used to investigate hypothetical climate change scenarios, such as changes to sea level, wave climate, or reef roughness due to coral degradation or restoration. Shope et al. (2016) used the formulation of Stockdon et al. (2006) (developed on the basis of runup data obtained on sandy sloping beaches under nonextreme offshore forcing) to estimate Pacific island runup under future climate change scenarios. The BEWARE system developed for this study could provide a more comprehensive estimate than those based on the Stockdon et al. (2006) equations by accounting for input uncertainty and considering the full suite of processes involved in reef hydrodynamics (including resonance) and the resulting wave-driven flooding.

The reaction to climate change does not have to be passive—mitigating measures can be taken by affected island communities to improve resilience to flooding. The value of coral reefs as nature-based flood defenses can also be analyzed with this model and used to prioritize conservation or restoration efforts. Ferrario et al. (2014) demonstrated that reef restoration is a more cost-effective solution for coastal risk reduction on coral reef-lined islands than the construction of artificial breakwaters. Given the scarce resources available for such projects, the BEWARE system can be used to understand which coral reef-lined areas are most vulnerable and where coral restoration can provide the largest return in terms of coastal hazard risk reduction.

Since reef roughness is correlated to its coral health (Baldock et al., 2014), degradation of coral due to bleaching or ocean acidification may reduce its ability to effectively dissipate wave energy (Sheppard et al., 2005; Quataert et al., 2015). Conversely, restoration efforts that improve coral ecosystem quality (Fox et al., 2005; Haisfield et al., 2010) may increase roughness and thus provide more effective wave attenuation. The health of reef ecosystems under different climate change or restoration scenarios could be accounted for by examining a given location's sensitivity to c_f in the model. It is thus possible that significant increases in roughness brought on by reef restoration could help offset some of the effects of sea level rise on wave-induced flooding.

Although the LLR analysis (Figure 10) suggests that c_f is a less important parameter than W_{reef} for determining wave transformation and the resulting water levels, it should be noted that it is easier to influence c_f by coral restoration than it is to change W_{reef}. Thus, restoration is a viable strategy for flood risk reduction on coral reef-lined islands.

5. Conclusions

The "Bayesian Estimator for Wave Attack in Reef Environments" (BEWARE) system for estimating flooding hazards on coral reef-lined coasts was developed by training a Bayesian network with a synthetic database generated by XBeach Non-Hydrostatic (XBNH) model simulations. The XBNH process-based numerical wave and water level model is shown to be capable of reproducing wave transformation processes on fringing reefs, including resonant reef flat amplification. BEWARE improves system understanding of reef hydrodynamics, building on previous work by examining the intrinsic and extrinsic factors controlling runup on reef-lined coasts.

BEWARE shows high predictive skill for flooding conditions from the XBNH model, and was validated for a limited number of case studies. Using the log likelihood ratio test, it was found that offshore wave conditions, water level, and reef width are the most important parameters required to estimate extreme water levels and runup on reef-fronted coasts using a Bayesian network, whereas having knowledge of the reef roughness or beach slope appears less important.

BEWARE has the potential to form the basis for early warning systems and scenario assessment applications on reef-lined coasts. The applicability of the BEWARE system can be further enhanced if supplemented by key parameters (e.g., reef flat width) obtained from remote sensing platforms as well as field measurements of reef hydrodynamics.

References

Baldock, T. E., Golshani, A., Callaghan, D. P., Saunders, M. I., & Mumby, P. J. (2014). Impact of sea-level rise and coral mortality on the wave dynamics and wave forces on barrier reefs. *Marine Pollution Bulletin*, *83*(1), 155–164. https://doi.org/10.1016/j.marpolbul.2014.03.058

Bayes, T., & Price, M. (1763). An essay towards solving a problem in the doctrine of chances. *Philosophical Transactions of the Royal Society of London*, *53*, 370–418. https://doi.org/10.1093/biomet/45.3-4.293

Becker, J. M., Merrifield, M. A., & Ford, M. (2014). Water level effects on breaking wave setup for Pacific Island fringing reefs. *Journal of Geophysical Research: Ocean*, *119*, 914–932. https://doi.org/10.1002/2013JC009373

Beetham, E. P., Kench, P. S., O'callaghan, J., & Popinet, S. (2015). Wave transformation and shoreline water level on Funafuti Atoll, Tuvalu. *Journal of Geophysical Research: Ocean*, *120*, 1–16. https://doi.org/10.1002/2014JC010472

Bosserelle, C., Kruger, J., Movono, M., & Reddy, S. (2015). Wave inundation on the Coral Coast of Fiji. In *Australasian coasts & ports conference 2015* (pp. 96–101). Auckland, New Zealand: Engineers Australia and IPENZ.

Brocchini, M., & Baldock, T. E. (2008). Recent advances in modeling swash zone dynamics: Influence of surf-swash interaction on nearshore hydrodynamics and morphodynamics. *Reviews of Geophysics*, *46*, RG3003. https://doi.org/10.1029/2006RG000215

Cheriton, O. M., Storlazzi, C. D., & Rosenberger, K. J. (2016). Observations of wave transformation over a fringing coral reef and the importance of low-frequency waves and offshore water levels to runup, overwash, and coastal flooding. *Journal of Geophysical Research: Ocean*, *121*, 3121–3140. https://doi.org/10.1002/2015JC011231

Demirbilek, Z., Nwogu, O., & Ward, D. (2007). Laboratory study of wind effect on runup over fringing reefs (Tech. Rep. ERDC/CHL TR-07–8). Washington, DC: U.S. Army Corps of Engineers.

Ferrario, F., Beck, M. W., Storlazzi, C. D., Micheli, F., Shepard, C. C., & Airoldi, L. (2014). The effectiveness of coral reefs for coastal hazard risk reduction and adaptation. *Nature Communications*, *5*(May), 1–9. https://doi.org/10.1038/ncomms4794

Fletcher, C. H., & Richmond, B. M. (2010). *Climate change in the Federated States of Micronesia: Food and water security, climate risk management, and adaptive strategies* (report). Honolulu: University of Hawai'i.

Fox, H. E., Mous, P. J., Pet, J. S., Muljadi, A. H., & Caldwell, R. L. (2005). Experimental assessment of coral reef rehabilitation following blast fishing. *Conservation Biology*, *19*(1), 98–107. https://doi.org/10.1111/j.1523-1739.2005.00261.x

Gawehn, M., van Dongeren, A. R., van Rooijen, A., Storlazzi, C. D., Cheriton, O. M., & Reniers, A. J. H. M. (2016). Identification and classification of very low frequency waves on a coral reef flat. *Journal of Geophysical Research: Ocean*, *121*, 7560–7574. https://doi.org/10.1002/2016JC011834

Gingerich, S. B., Voss, C. I., & Johnson, A. G. (2017). Seawater-flooding events and impact on freshwater lenses of low-lying islands: Controlling factors, basic management and mitigation. *Journal of Hydrology*, *551*, 676–688. https://doi.org/10.1016/j.jhydrol.2017.03.001

Gutierrez, B. T., Plant, N. G., & Thieler, E. R. (2011). A Bayesian network to predict coastal vulnerability to sea level rise. *Journal of Geophysical Research*, *116*, F02009. https://doi.org/10.1029/2010JF001891

Gutierrez, B. T., Plant, N. G., Thieler, E. R., & Turecek, A. (2015). Using a Bayesian network to predict barrier island geomorphologic characteristics. *Journal of Geophysical Research: Earth Surface*, *120*, 2452–2475. https://doi.org/10.1002/2014JF003270

Haisfield, K. M., Fox, H. E., Yen, S., Mangubhai, S., & Mous, P. J. (2010). An ounce of prevention: Cost-effectiveness of coral reef rehabilitation relative to enforcement. *Conservation Letters*, *3*(4), 243–250. https://doi.org/10.1111/j.1755-263X.2010.00104.x

Hinkel, J., Lincke, D., Vafeidis, A. T., Perrette, M., Nicholls, R. J., Tol, R. S. J., . . . Levermann, A. (2014). Coastal flood damage and adaptation costs under 21st century sea-level rise. *Proceedings of the National Academy of Sciences of the United States of America*, *111*(9), 3292–3297. https://doi.org/10.1073/pnas.1222469111

Hirschberg, P. A., Abrams, E., Bleistein, A., Bua, W., Monache, L. D., Dulong, T. W., . . . Stuart, N. (2011). A weather and climate enterprise strategic implementation plan for generating and communicating forecast uncertainty information. *Bulletin of the American Meteorological Society*, *92*(12), 1651–1666. https://doi.org/10.1175/BAMS-D-11-00073.1

Hoeke, R. K., McInnes, K., Kruger, J., McNaught, R. J., Hunter, J. R., & Smithers, S. G. (2013). Widespread inundation of Pacific islands triggered by distant-source wind-waves. *Global and Planetary Change*, *108*, 128–138. https://doi.org/10.1016/j.gloplacha.2013.06.006

Jäger, W. S., Christie, E. K., Hanea, A., Den Heijer, M. C., & Spencer, T. (2017). A Bayesian network approach for coastal risk analysis and decision making. *Coastal Engineering*, https://doi.org/10.1016/j.coastaleng.2017.05.004. Retrieved from http://www.sciencedirect.com/science/article/pii/S0378383917300625.

Jäger, W. S., den Heijer, C., Bolle, A., & Hanea, A. (2015). A Bayesian network approach to coastal storm impact modeling. Paper presented at 12th international conference on applications of statistics and probability in civil engineering, University of British Columbia, Vancouver, BC.

Matias, A., Williams, J. J., Masselink, G., & Ferreira, O. (2012). Overwash threshold for gravel barriers. *Coastal Engineering*, *63*, 48–61. https://doi.org/10.1016/j.coastaleng.2011.12.006

McCall, R. T., Masselink, G., Poate, T. G., Roelvink, J. A., Almeida, L. P., Davidson, M., & Russell, P. E. (2014). Modelling storm hydrodynamics on gravel beaches with XBeach-G. *Coastal Engineering*, *91*, 231–250. https://doi.org/10.1016/j.coastaleng.2014.06.007

Meheux, K., Dominey-Howes, D., & Lloyd, K. (2007). Natural hazard impacts in small island developing states: A review of current knowledge and future research needs, *Natural Hazards*, *40*(2), 429–446. https://doi.org/10.1007/s11069-006-9001-5

Merrifield, M. A., Becker, J. M., Ford, M., & Yao, Y. (2014). Observations and estimates of wave-driven water level extremes at the Marshall Islands. *Geophysical Research Letters*, *41*, 7245–7253. https://doi.org/10.1002/2014GL061005

Nakaza, E., Tsukayama, S., & Hino, M. (1990). Bore-like surf beat on reef coasts. In *Proceedings of 22nd international conference on coastal engineering* (pp. 743–756). Reston, VA: American Society of Civil Engineers.

Nicholls, R. J., & Cazenave, A. (2010). Sea level rise and its impact on coastal zones, *Science*, *328*(2010), 1517–1520. https://doi.org/10.1126/science.1185782

Norsys. (2003). *Netica—Application for belief networks and influence diagrams: User's guide*. Vancouver, BC: Author.

Nwogu, O., & Demirbilek, Z. (2010). Infragravity wave motions and runup over shallow fringing reefs. *Journal of Waterway, Port, Coastal, and Ocean Engineering*, *136*(December), 295–305. https://doi.org/10.1061/(ASCE)WW.1943-5460.0000050

Owen, S. D., Kench, P. S., & Ford, M. (2016). Improving understanding of the spatial dimensions of biophysical change in atoll island countries and implications for island communities: A Marshall Islands' case study. *Applied Geography*, *72*, 55–64. https://doi.org/10.1016/j.apgeog.2016.05.004

Péquignet, A.-C., Becker, J. M., Merrifield, M. A., & Aucan, J. (2009). Forcing of resonant modes on a fringing reef during tropical storm Man-Yi. *Geophysical Research Letters*, *36*, L03607. https://doi.org/10.1029/2008GL036259

Péquignet, A.-C., Becker, J. M., Merrifield, M. A., & Boc, S. J. (2011). The dissipation of wind wave energy across a fringing reef at Ipan, Guam. *Coral Reefs*, *30*(Suppl. 1), 71–82. https://doi.org/10.1007/s00338-011-0719-5

Plant, N. G., & Holland, K. T. (2011). Prediction and assimilation of surf-zone processes using a Bayesian network. Part I: Forward models. *Coastal Engineering*, *58*(1), 119–130. https://doi.org/10.1016/j.coastaleng.2010.09.003

Poelhekke, L., Jäger, W. S., van Dongeren, A. R., Plomaritis, T. A., McCall, R. T., & Ferreira, O. (2016). Predicting coastal hazards for sandy coasts with a Bayesian network. *Coastal Engineering*, *118*, 21–34. https://doi.org/10.1016/j.coastaleng.2016.08.011

Pomeroy, A., Lowe, R. J., Symonds, G., van Dongeren, A. R., & Moore, C. (2012b). The dynamics of infragravity wave transformation over a fringing reef. *Journal of Geophysical Research*, *117*, C11022. https://doi.org/10.1029/2012JC008310

Pomeroy, A., van Dongeren, A. R., Lowe, R. J., van Thiel de Vries, J. S. M., & Roelvink, J. A. (2012a). Low-frequency wave resonance in fringing reef environments. *Coastal Engineering Proceedings*, *2012*, 1–10.

Quataert, E., Storlazzi, C. D., van Rooijen, A., Cheriton, O. M., & van Dongeren, A. R. (2015). The influence of coral reefs and climate change on wave-driven flooding of tropical coastlines. *Geophysical Research Letters*, *42*, 6407–6415. https://doi.org/10.1002/2015GL064861

Roeber, V., & Bricker, J. D. (2015). Destructive tsunami-like wave generated by surf beat over a coral reef during Typhoon Haiyan. *Nature Communications*, *6*, 7854. https://doi.org/10.1038/ncomms8854

Roelvink, J. A., van Dongeren, A. R., McCall, R., Hoonhout, T., van Rooijen, B., van Geer, A., . . . Quataert, E. (2015). *XBeach technical reference: Kingsday release* (technical report). Delft, the Netherlands: Deltares.

Sheppard, C., Dixon, D. J., Gourlay, M. R., Sheppard, A., Payet, R., & Sheppard, C. (2005). Coral mortality increases wave energy reaching shores protected by reef flats: Examples from the Seychelles. *Estuarine, Coastal and Shelf Science*, *64*(2–3), 223–234. https://doi.org/10.1016/j.ecss.2005.02.016

Shimozono, T., Tajima, Y., Kennedy, A. B., Nobuoka, H., Sasaki, J., & Sato, S. (2015). Combined infragravity wave and sea-swell runup over fringing reefs by super typhoon Haiyan. *Journal of Geophysical Research: Ocean*, *120*, 4463–4486. https://doi.org/10.1002/2015JC010760

Shope, J. B., Storlazzi, C. D., Erikson, L. H., & Hegermiller, C. A. (2016). Changes to extreme wave climates of islands within the Western Tropical Pacific throughout the 21st century under RCP 4.5 and RCP 8.5, with implications for island vulnerability and sustainability. *Global and Planetary Change*, *141*, 25–38. https://doi.org/10.1016/j.gloplacha.2016.03.009

Smit, P. B., Roelvink, J. A., van Thiel de Vries, J. S. M., McCall, R. T., van Dongeren, A. R., & Zwinkels, J. R. (2014). *XBeach: Non-hydrostatic model*. Delft, The Netherlands: Delft University of Technology.

Stockdon, H. F., Holman, R. A., Howd, P. A., & Sallenger, A. H. (2006). Empirical parameterization of setup, swash, and runup. *Coastal Engineering*, *53*(7), 573–588. https://doi.org/10.1016/j.coastaleng.2005.12.005

Storlazzi, C. D., Elias, E. P. L., & Berkowitz, P. (2015). Many atolls may be uninhabitable within decades due to climate change. *Scientific Reports*, *5*, 14546. https://doi.org/10.1038/srep14546

Storlazzi, C. D., Elias, E. P. L., Field, M. E., & Presto, M. K. (2011). Numerical modeling of the impact of sea-level rise on fringing coral reef hydrodynamics and sediment transport. *Coral Reefs*, *30*(Suppl. 1), 83–96. https://doi.org/10.1007/s00338-011-0723-9

Symonds, G., Huntley, D. A., & Bowen, A. J. (1982). Two-dimensional surf beat: Long wave generation by a time-varying breakpoint. *Journal of Geophysical Research*, *87*(C1), 492–498. https://doi.org/10.1029/JC087iC01p00492

Tajima, Y., Shimozono, T., Gunasekara, K. H., & Cruz, E. C. (2016). Study on locally varying inundation characteristics induced by super typhoon Haiyan part 2: Deformation of storm waves on the beach with fringing reef along the east coast of Eastern Samar. *Coastal Engineering Journal*, *58*(1), 1640003. https://doi.org/10.1142/S0578563416400039

Terry, J. P., & Falkland, A. C. (2010). Responses of atoll freshwater lenses to storm-surge overwash in the Northern Cook Islands. *Hydrogeology Journal*, *18*(3), 749–759. https://doi.org/10.1007/s10040-009-0544-x

Tolman, H. L. (2009). *User manual and system documentation of WAVEWATCH-III™ version 3.14* (technical note). Camp Springs, MD: U. S. Department of Commerce.

UN-Habitat. (2015). *Urbanization and climate change in small island developing states*. Nairobi, Kenya: Author.

UNISDR. (2015). *Sendai framework for disaster risk reduction 2015–2030*. Sendai, Japan: Author.

U.S. Fish and Wildlife Service. (2015). U.S. Fish and Wildlife Service pacific region. Retrieved from https://www.fws.gov/pacific/

van Rijn, L. C. (2011). *Principles of fluid flow and surface waves in rivers, estuaries, seas and oceans*. Amsterdam, The Netherlands: Aqua Publications.

van Verseveld, H. C. W., van Dongeren, A. R., Plant, N. G., Jäger, W. S., & den Heijer, C. (2015). Modelling multi-hazard hurricane damages on an urbanized coast with a Bayesian Network approach. *Coastal Engineering*, *103*, 1–14. https://doi.org/10.1016/j.coastaleng.2015.05.006

Vetter, O., Becker, J. M., Merrifield, M. A., Péquignet, A.-C., Aucan, J., Boc, S. J., & Pollock, C. E. (2010). Wave setup over a Pacific Island fringing reef. *Journal of Geophysical Research*, *115*, C12066. https://doi.org/10.1029/2010JC006455

Zijlema, M. (2012). Modelling wave transformation across a fringing reef using SWASH. *Coastal Engineering*, *2012*, 1–12. https://doi.org/10.9753/icce.v33.currents.26